The Astrophysical Journal Letters, 958:L36 (6pp), 2023 December 1 https://doi.org/10.3847/2041-8213/ad0b0c

An Extended Lyα Outflow from a Radio Galaxy at $z = 3.7$?

Miguel Coloma Puga[1,2], Barbara Balmaverde[2], Alessandro Capetti[2], Francesco Massaro[1], Cristina Ramos Almeida[3,4], George Miley[5], Roberto Gilli[6], and Alessandro Marconi[7,8]
[1] Department of Physics, Università di Torino Via Pietro Giuria, 1, I-10125, Torino, Italy
[2] INAF—Osservatorio Astrofisico di Torino Via Osservatorio 20, I-10025 Pino Torinese, Italy
[3] Instituto de Astrofisica de Canarias C. Vía Láctea, s/n, E-38205 La Laguna, Tenerife, Spain
[4] Departamento de Astrofísica, Universidad de La Laguna E-38206, La Laguna, Tenerife, Spain
[5] Leiden Observatory, Leiden University PO Box 9513, 2300 RA Leiden, The Netherlands
[6] Osservatorio di Astrofisica e Scienza dello Spazio di Bologna Via Gobetti 93/3, I-40129 Bologna, Italy
[7] Dipartimento di Fisica e Astronomia, Università degli Studi di Firenze Via G. Sansone 1, I-50019, Sesto Fiorentino, Firenze, Italy
[8] INAF—Osservatorio Astrofisico di Arcetri Largo E. Fermi 5, I-50125, Firenze, Italy
Received 2023 July 28; revised 2023 November 7; accepted 2023 November 9; published 2023 November 30

Abstract

Spatially resolved observations of active galactic nuclei (AGN) host galaxies undergoing feedback processes are one of the most relevant avenues through which galactic evolution can be studied, given the long-lasting effects AGN feedback has on gas reservoirs, star formation, and AGN environments at all scales. Within this context, we report results from Very Large Telescope/MUSE integral field optical spectroscopy of TN J1049-1258, one of the most powerful radio sources known, at a redshift of 3.7. We detected extended (~18 kpc) Lyα emission, spatially aligned with the radio axis, redshifted by 2250 ± 60 km s^{-1} with respect to the host galaxy systemic velocity, and cospatial with UV continuum emission. This Lyα emission could arise from a companion galaxy, although there are arguments against this interpretation. Alternatively, it might correspond to an outflow of ionized gas stemming from the radio galaxy. The outflow would be the highest redshift spatially resolved ionized outflow to date. The enormous amount of energy injected, however, appears to be unable to quench the host galaxy's prodigious star formation, occurring at a rate of ~4500 $M_{\odot}$yr^{-1}, estimated using its far-infrared luminosity. Within the field, we also found two companion galaxies at projected distances of ~25 and ~60 kpc from the host, which suggests the host galaxy is harbored within a protocluster.

Unified Astronomy Thesaurus concepts: High-redshift galaxy clusters (2007); Radio galaxies (1343); Active galactic nuclei (16); Radio jets (1347)

1. Introduction

Outflows are believed to be the main driver through which active galactic nuclei (AGN) regulate the evolution of their host galaxies and affect the large-scale environment (AGN feedback), operating mostly at the epoch of the peak of star formation between redshift 2 and 3 (Hopkins 2006; Miley & De Breuck 2008). Outflows, extended on kiloparsec scales, powered by the AGN radiative pressure (quasar feedback mode) and/or radio jets (radio feedback mode), have been resolved in ionized, atomic, and molecular gas both in local (e.g., Rupke & Veilleux 2011; Cicone et al. 2012; Rodriguez Zaurin et al. 2013; Rupke & Veilleux 2013; Speranza et al. 2021; Ramos Almeida et al. 2022) and in high-redshift (radio-loud and radio-quiet) quasars (e.g., Alexander et al. 2010; Nesvadba et al. 2010; Maiolino et al. 2012; Cano-Díaz et al. 2012; Cresci et al. 2015). Characterizing and constraining the effects and extent to which AGN feedback affects star formation is one of the most important problems in modern astrophysics, as it has ties to the biggest questions in galaxy evolution and cosmology.

In this context, high-redshift radio galaxies (HzRGs) are particularly relevant as the nuclear regions are obscured along our line of sight due to a circumnuclear dusty structure (e.g., Antonucci 1993) or by the host galaxy itself. The lower nuclear continuum luminosities allow us to reduce the observational uncertainties produced by the subtraction of a prominent point-spread function (PSF), probing the host and the gas structure down to the limit of the spatial resolution of only a few kiloparsecs.

We started a comprehensive program of observations with the Multi Unit Spectroscopic Explorer (MUSE) at the Very Large Telescope to explore the properties of the ionized gas in HzRGs. In this Letter, we present the results obtained for TN J1049-1258, an HzRG at redshift 3.697 ± 0.004 (Bornancini et al. 2007), located at $\alpha = 10{:}49{:}06.2$, $\delta = -12{:}58{:}19$ (J2000). The scale factor at this redshift (assuming an $H_0 = 69.6$ and $\Omega_m = 0.286$ cosmology) is 7.3 kpc arcsec^{-1}. Its radio flux measured at 74 MHz by the NRAO Very Large Array (VLA) Sky Survey is 5.18 ± 0.56 Jy while its radio spectral index is $\alpha = 1.4$ (Condon et al. 1998).[9] The jet power, $P_{\rm jet}$, can be obtained using the correlation between $P_{\rm jet}$ and radio luminosity, based on the measurement of the mechanical power of radio sources producing cavities in the surrounding hot gas as proposed by Cavagnolo et al. (2010). The radio luminosity of TN J1049-1258 at (rest frame) 327 MHz can be estimated as $P_{327} = 2.7 \times 10^{44}$ erg s^{-1}, which yields a jet power of $P_{\rm jet} \sim 6 \times 10^{45}$ erg s^{-1}. A similar value is obtained by using the relation between radio and jet power from Willott et al. (1999). In the Karl G. Jansky VLA Sky Survey (Lacy et al. 2020), performed at 3 GHz with a resolution of 2.″5, its radio emission is dominated by two radio components

[9] Spectral index, α, is defined by flux density, $S_\nu \propto \nu^{-\alpha}$.

separated by 11″ (80 kpc) oriented at the position angle −80°, with the host located close to their midpoint. Its radio luminosity at the rest-frame frequency of 500 MHz is 8.7×10^{28} W Hz^{-1}, making TN J1049-1258 one of the most luminous radio sources known (see Miley & De Breuck 2008). The flux at 3.5 μm, corresponding to the optical emission in the rest frame, measured by Wide-field Infrared Survey Explorer (WISE; Wright et al. 2010) of TN J1049-1258 indicates a luminosity of $2 \times 10^{11} L_{\odot}$, suggesting that its host is already a very massive galaxy.

2. Observations and Data Analysis

The observations were carried out with the Multi Unit Spectroscopic Explorer (MUSE) on 2022 January 29 as part of the program ID:108.22FU. Four separate observations were performed, between which the telescope was rotated 90° to reject cosmic rays, for a total of 2800 s of exposure time. The seeing measured from several point sources in the field of view was estimated as $0\farcs71 \pm 0\farcs04$. We used the ESO MUSE pipeline (version 2.8.7) to obtain a fully reduced and calibrated data cube (Weilbacher et al. 2020). We derived an absolute astrometric calibration of the MUSE data by cross-matching visible sources in both MUSE and Panoramic Survey and Rapid Response System (Pan-STARRS; Chambers et al. 2016). Based on the scatter of the sources considered, we estimate the derived astrometry to have an error of ∼0.″2.

After first inspecting the nuclear spectrum on a large aperture around the peak of Lyα emission, we found two emission lines separated by about 50 Å. To fully characterize both the emission line morphology and the gas kinematics, we then performed a two Gaussian component fit in each spaxel (see Figure 1 for the nuclear and off-nuclear spectra). Aiming to increase the signal-to-noise ratio (S/N) per pixel, the cube was spatially rebinned into 2×2 pixels, resulting in a $0\farcs4 \times 0\farcs4$ area. The *modeling* tool from *Astropy*'s Python package (Astropy Collaboration et al. 2013, 2018; Price-Whelan et al. 2022) was used to model and fit both the continuum and emission lines. For the continuum, we used a linear least squares fit, while the emission lines were modeled with a Gaussian using a Levenberg–Marquardt least squares fit.

From the fit, we obtained the distribution of total flux and first and second moments for both components, while the uncertainties of the parameters were obtained through a Monte Carlo simulation. Each realization consists of adding flux variations to each spectral pixel, with the value of the variations taken at random from a normal distribution centered at the pixel noise. From each realization, a value for the relevant parameters (line center, amplitude, width) is obtained. After a set number of iterations (100 in our case) we obtain a value distribution for each of these parameters, from which we extract the mean (parameter value) and 1σ standard deviation (parameter uncertainty). The pixel noise was calculated as the 1σ standard deviation of the flux in a 50 nm interval centered on Lyα from a section of empty sky of equal size as the cube extracted for the line analysis (80×80 pixels or $16'' \times 16''$). All emission line maps have been obtained by setting a signal-to-noise threshold at 3.

The continuum map was obtained using multiple intervals within MUSE's wavelength range (475–935 nm, 101–198 nm rest frame) over a total range of 144 nm, selected to avoid both sky lines as well as object emission lines.

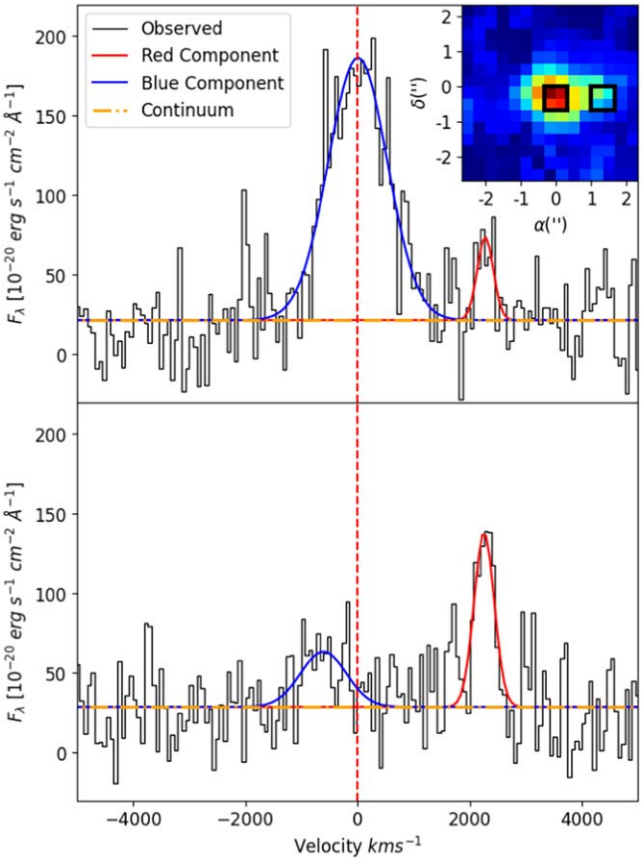

Figure 1. Top: nuclear spectrum of TN J1049-1258, extracted from a $0\farcs8 \times 0\farcs8$ synthetic aperture, along with the modeled continuum and fitted lines. The spectrum shows the presence of two components, separated by ∼2250 km s^{-1}. In the top right inset, we show the total Lyα flux map, spatially rebinned into 2×2 pixels, with the two synthetic apertures used to extract the nuclear and off-nuclear spectra superimposed. Bottom: off-nuclear spectrum extracted 1.″6 west of the nucleus. The redshifted line becomes the brightest component. In both cases, the red dashed line marks the host galaxy's systemic velocity, corresponding to a redshift of 3.697. The X and Y scales are identical in both spectra.

3. Results

We estimated the redshift of TN J1049-1258 from the fit of the main component of Lyα line in the nuclear spectrum, which corresponded to $z = 3.697 \pm 0.001$, the same value obtained by Bornancini et al. (2007). However, it must be noted that the Lyα line peak has been observed to be redshifted from the systemic velocity (measured by the Hα emission) by ∼450 km s^{-1} on average, and by as much as ∼900 km s^{-1} (e.g., Steidel et al. 2010).

The emission maps of both components and all relevant velocity and velocity dispersion maps are shown in Figure 2. The velocity field estimated from the host galaxy's Lyα emission presents a large gradient, with a velocity range of ∼900 km s^{-1} and a velocity dispersion ranging from 500 to 1500 km s^{-1}, that can be ascribed to either rotation or radial motion. While there is a clear spatial correlation between width and relative velocity, interpreting the absolute values of the velocity dispersion is made difficult by the resonant character of Lyα emission. Neutral hydrogen in the line of sight of the emitting gas will result in peaks and troughs, deeply modifying the original line profile depending on the density, distribution, and velocity of the neutral H gas.

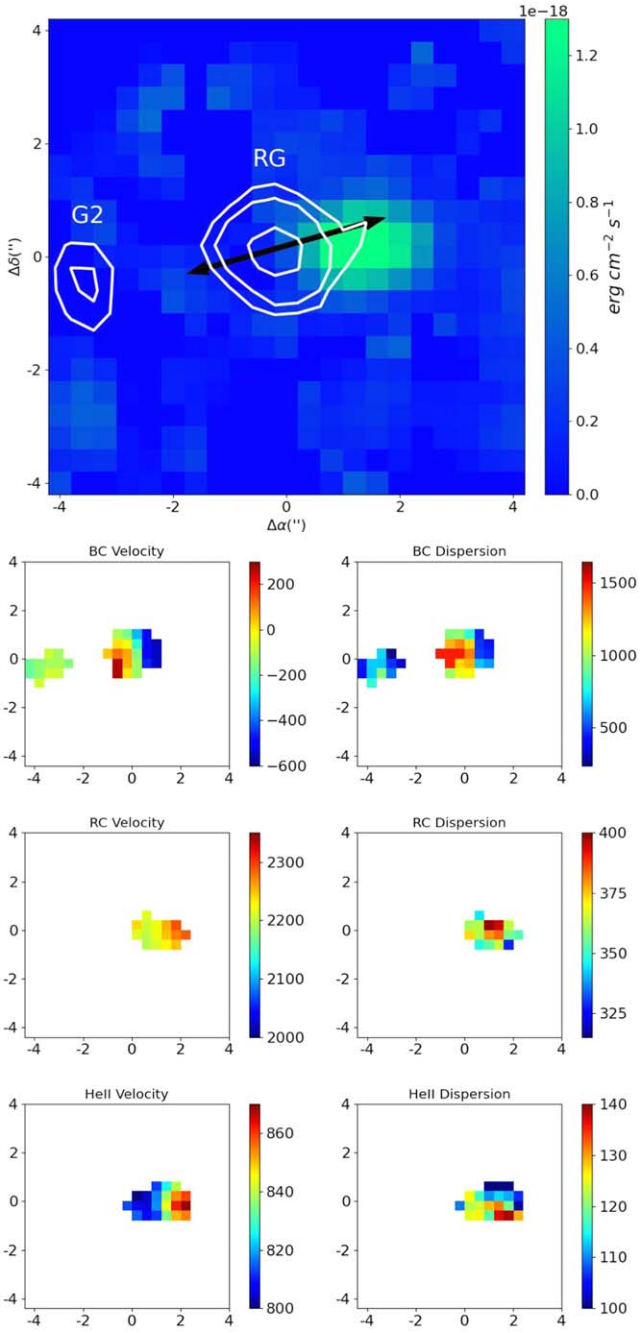

Figure 2. Top: Lyα emission map of the red component, with superimposed isointensity contours of the Lyα from the host galaxy. The field of view is ∼30 ×30 kpc. There is a clear offset between the center of the host galaxy emission and of the red component. A second source of Lyα emission (that we name G2) is seen ∼3.″5 east of the host galaxy. The arrow shows the radio axis. Bottom: maps of projected velocity and velocity dispersion of the host galaxy (top), of the red Lyα component (middle), and of the HeII line in km s^{-1}. In all cases, the signal-to-noise threshold on the line fit is set at 3σ.

The redshifted component has an elongated structure extending ∼2.″5, i.e., ∼18.5 kpc, measured as the distance between the two farthest pixels with S/N>3, along the same position angle of the radio structure. Its relative velocity, measured using the line profile in the off-nuclear spectrum (see Figure 1) is $v = 2250 \pm 60$ km s^{-1} and it remains remarkably similar throughout the spatial extent of the emission zone. In a similar fashion, the velocity dispersion values are within a range of ∼70 km s^{-1}, with this red component being much

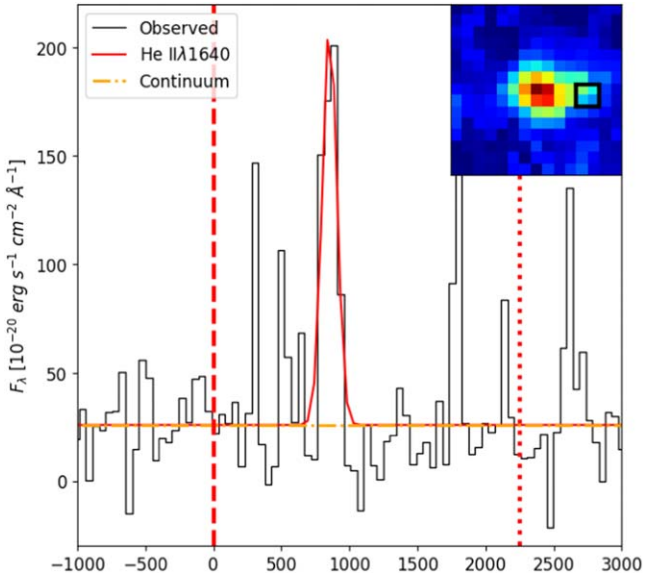

Figure 3. He II spectrum extracted using the same off-nuclear aperture as Lyα. The dashed line marks the host systemic velocity, and the dotted line marks the extended emission velocity.

narrower than the one in the host galaxy; its FWHM measured from the off-nuclear spectrum is $\sigma_{RC} = 430 \pm 20$ km s^{-1}.

In the region cospatial to the Lyα red component we also detected emission from the He IIλ1640 line (see Figure 3). This line is blueshifted by 1404 ± 9 km s^{-1} (value obtained from the off-nuclear spectrum shown in Figure 1) with respect to the Lyα emission. Its velocity and velocity dispersion maps are shown in Figure 2. From this spectrum. we obtain a line ratio Lyα/He II $= 1.5 \pm 0.3$, which is at the very low end of the values measured in HzRGs (see Villar-Martín et al. 2007).

UV continuum emission, within the rest-frame range ∼1000–2000 Å, (see Figure 4) is observed on the west side of the host galaxy, cospatial with the Lyα red component. The source observed ∼5″ south of the radio galaxy (RG from hereon) is a galaxy at $z = 0.87$, based on the identification of the [O II]$\lambda\lambda$ 3726,3729 doublet as well as Hδ and Hγ in its spectrum. The brightest UV source in the field is another potential companion we named G1, located ∼8″ (∼60 kpc) southeast of the host galaxy. Its Lyα emission was detected at a very similar redshift (see Figure 5, top panel) and its high-redshift identification is also supported by it being a g-dropout based on the photometry from Pan-STARRS (Chambers et al. 2016).[10]

To the east of the radio galaxy, another patch of Lyα emission can be seen in the top panel of Figure 2. This is associated with a companion galaxy we named G2, whose identification is possible thanks to the presence of Lyα (see Figure 5, bottom panel), He IIλ1640, and C IV $\lambda\lambda$1548, 1550 in its spectrum. Its redshift, $z = 3.685 \pm 0.002$, was estimated from the He IIλ1640 emission, which is a nonresonant line. The presence of G1 and G2 suggests TN J1049-1258 may be harbored within a protocluster.

The main result of these observations is the presence of extended Lyα emission redshifted by ∼2250 km s^{-1} and we can envisage two possibilities for its origin:

[10] The Pan-STARRS aperture magnitudes for G1 are $g = 24.08 \pm 0.02$, $r = 22.44 \pm 0.01$, and $i = 22.39 \pm 0.01$, respectively, then satisfying the g-dropout criteria by Pouliasis et al. (2022).

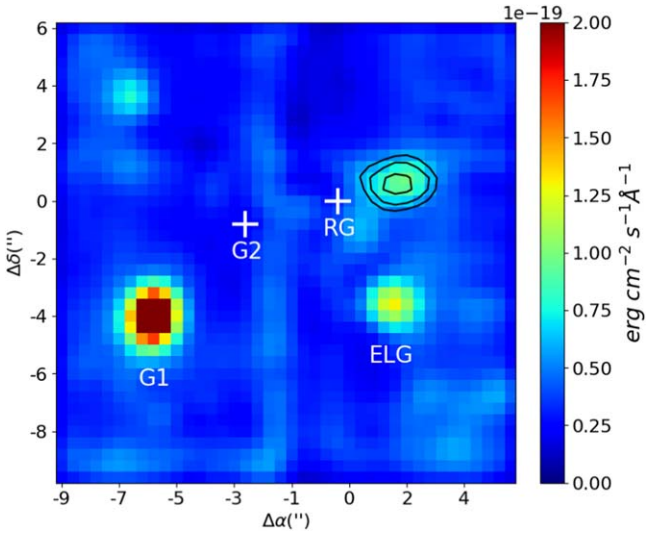

Figure 4. Rest frame UV continuum flux density map of the field around TN J1049-1258. A source of continuum can be seen to the west of the Lyα emission center, cospatial with the red component (black contours at 0.5, 0.8. and 1.3 10^{-18} erg cm^{-2} s^{-1}). The brightest UV source, G1, is located $\sim 8''$ ($\sim$60 kpc) southeast of the host galaxy. At the location of G2 (marked with a "+" sign) an image defect (the vertical line at $\Delta\alpha \sim -1$") does not allow us to obtain a robust UV counterpart to the Lyα emission seen in Figure 2. Another source found $5''$ to the south and slightly west is identified as a $z = 0.87$ emission line galaxy and labeled ELG.

(1) A companion galaxy. The presence of UV continuum emission cospatial with the Lyα region suggests that this might be associated with another galaxy at a similar redshift. This interpretation is also supported by the low velocity dispersion ($\sigma = 430 \pm 20$ km s^{-1}) of the Lyα emission. The Lyα equivalent width (EW) of 6.6 ± 2.0 Å does not provide useful information as to the origin of the line emission since the EW of Lyman alpha emitters spans a considerably wide range, with measurements ranging from a few angstroms to several hundreds (see Kerutt et al. 2022). However, studies of high-redshift galaxies found that the typical radius of a $z \sim 4$ galaxy is $0\farcs2$, that is, 1.5 kpc (Bouwens et al. 2004; Ferguson et al. 2004). The FWHM of the Lyα red component emission is significantly larger: by fitting its spatial distribution with a Gaussian we obtain a size of $1\farcs79 \pm 0\farcs14$, equivalent to a deconvolved extension of $R = 12.0 \pm 0.9$ kpc. We must note, however, that G1 is also extended, with a deconvolved size of 7.3 ± 0.5 kpc. The strongest argument against this interpretation is the blueshift of $\sim$1400 km s^{-1}, which the He IIλ1640 line presents with respect to the extended Lyα line, as it greatly exceeds the range of velocity offsets between Lyα and nebular lines observed in high-redshift sources (Steidel et al. 2010), arguing in favor of a different origin.

(2) An outflow of ionized gas. This hypothesis is supported by simulations of the theoretical profile of Lyα (Ahn 2004; Verhamme et al. 2006; Behrens et al. 2014). In particular, the models by Behrens et al. (2014) show that a bipolar expanding shell, a reasonable approximation for a nuclear outflow, can produce a secondary redshifted peak. This unusual line profile is explained by the fact that Lyα is a resonant emission line, subject to the effects of radiative transfer due to the large cross-section of interaction between Lyα photons and neutral hydrogen atoms. As a consequence, the ubiquity of neutral hydrogen not only within galaxies but in the intergalactic medium along our line of sight prevents most, if not all, light

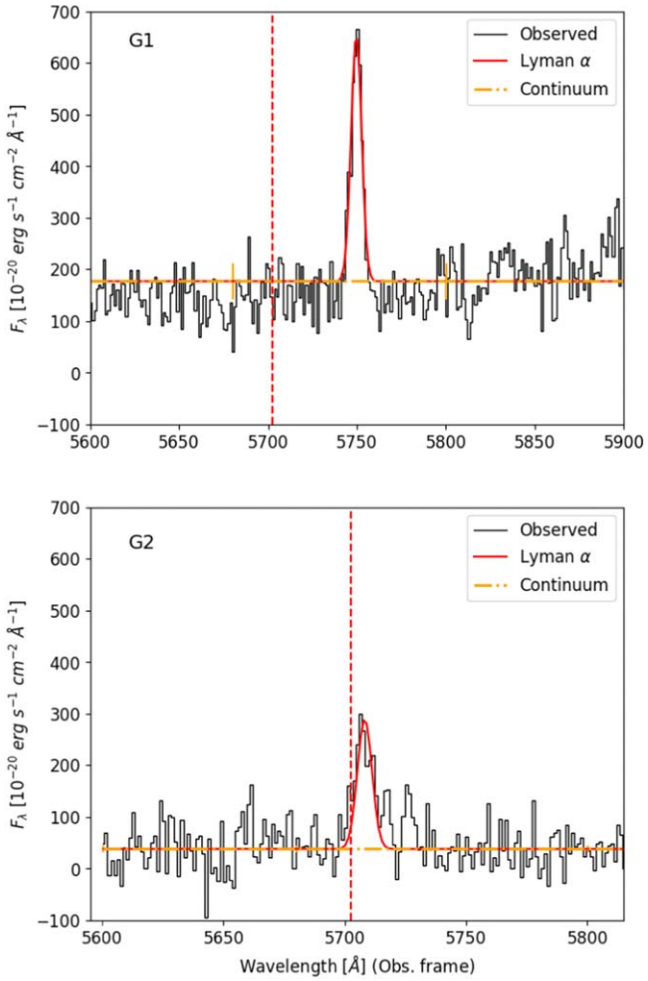

Figure 5. Spectra in the Lyα region for the two companion galaxies, G1 (top) and G2 (bottom). The red dashed line marks the RG's redshift measured with Lyα.

blueward of the central Lyα wavelength from emerging and, as is the case here, only the red side is observed. These effects can also explain the large velocity difference between the Lyα and the He II.

Additionally, the presence of UV continuum aligned with the radio axis is a common feature of HzRGs and has been explained as due to a combination of scattered nuclear light, fast shocks, and jet-induced star formation (see, e.g., McCarthy 1993 or Miley & De Breuck 2008), which also points to an in-host origin for the emission.

With all of these considerations taken into account, we conclude that the outflow hypothesis is the more plausible scenario.

We estimated the mass of the outflow, $M_{\rm out}$, from the Hβ luminosity, $L_{\rm H\beta}$, using the relation derived by Osterbrock (1989):

$$M_{\rm out} = 7.5 \times 10^{-3} \left(\frac{10^4}{n_e} \frac{L_{\rm H\beta}}{L_\odot} \right) M_\odot, \quad (1)$$

assuming the ratios Lyα/ H$\alpha = 8.7$ (Sobral & Matthee 2019) and Hα/H$\beta = 2.86$, and a gas density of $n_e = 200$ cm^{-3}, which enables a comparison between the energetics of this object and a sample of low redshift radio-loud AGN that utilizes this same value (Speranza et al. 2022).

We derived the following physical quantities (see, e.g., Fiore et al. 2017) for the outflow:

1. mass outflow rate: $\dot{M} = 3v_{\rm out}\frac{M_{\rm H\beta}}{R_{\rm out}} = 3.4 M_{\odot}\ {\rm yr}^{-1}$
2. kinetic energy: $\rm E_{kin} = \frac{1}{2}M_{H\beta}v_{out}^2 = 10^{56.6}$ erg
3. kinetic power $\dot{E}_{\rm kin} = \frac{1}{2}\dot{M}v_{\rm out}^2 = 10^{42.4}$ erg s^{-1}

where $v_{\rm out} = 2250$ km s^{-1} and $R_{\rm out} = 18.5$ kpc are the outflow velocity and full extension, respectively.

These estimates should be considered as lower limits for two reasons: first of all, we cannot correct for the effects of projection and, in addition, there might be a contribution of collisional excitation to the production of emission lines.

4. Discussion and Conclusions

The star formation rate (SFR) can be estimated from the UV and far-infrared emission of the source. While the UV light directly traces the young stellar population, the far-infrared emission is produced by warm dust heated by the UV photons emitted by young stars. We found the UV contribution to the SFR estimate for the RG to be negligible; it is also worth mentioning that UV continuum is subject to various effects that make it a more unreliable tracer at higher redshift (Wilkins et al. 2012).

Conversely, TN J1049-1258 has been detected by pointed far-infrared observations from the Spectral and Photometric Imaging Receiver onboard the Herschel satellite (Griffin et al. 2010; Poglitsch et al. 2010). At 250 and 350 μm, the observed fluxes are 63.0±9.5 and 67.7±11.8 mJy, respectively. These frequencies correspond to ∼50 and 70 μm in the rest frame, which coincides with the peak of the warm dust emission, heated by star-forming regions. Measurements from WISE were obtained on the W1 and W2 passbands (W3 and W4 were upper limits). From a fit to the spectral energy distribution using the WISE and Herschel measurements (see Balmaverde et al. 2016 for details) the derived total far-infrared luminosity is $L_{(8-1000\mu{\rm m})}$=$3.2\times10^{13}L_{\odot}$, which makes this source a hyperluminous infrared galaxy. It corresponds to a prodigious star formation rate of SFR∼4,500 $M_{\odot}$ yr^{-1}, among the highest values ever estimated (see the compilation of SFRs from Lagache et al. 2018). However, due to the low spatial resolving power of Herschel (the Herschel data reduction guide suggested to adopt an aperture photometry radius for the 250 and 350 μm images of 22″ and 30″, respectively), both companions and the $z = 0.87$ galaxy are included within the aperture, and thus there may be contamination from these sources. Additionally, there might be an AGN contribution. However, the torus emission peaks at 20–30 μm (Nenkova et al. 2008) and, in order to reproduce the far-infrared fluxes, this component would exceed the WISE measurements. We conclude that the AGN can only be a minor contributor to the Herschel fluxes.

Regarding the energetics of the system, the jet power is ∼4 orders of magnitude larger than the outflow kinetic power. Speranza et al. (2021) estimated the outflow kinetic power of a sample of radio galaxies at low redshift: while they measured values of $\dot{E_{\rm kin}}$ similar to that of TN J1049-1258, they found significantly larger values of $\dot{E_{\rm kin}}/P_{\rm jet}$, typically ∼0.1. This suggests that the relativistic jets and the outflow may be decoupled and produced by two independent acceleration mechanisms: the jets might be driven by the magnetic field in the innermost regions of the accretion disk, while the outflow is powered by radiation pressure. Alternatively, the ionized gas traced by the Lyα emission might just be the tip of the iceberg of a larger amount of outflowing gas, because this line is a poor tracer in terms of representative masses and luminosities. Dedicated radiative transfer simulations with geometries and parameters resembling those observed in TN 1049-1258 will be essential to fully model the results of these observations. To obtain a comprehensive view of the energetic of the outflow, we should also consider other ionized gas tracers, e.g., the optical [O III] line, unaffected by resonance and absorption effects. Moreover, a relevant contribution to the energetic of the outflow is expected to originate from the molecular gas component, which can be studied using lines produced by the CO molecule transitions or the [C ii]158 μm emission.

Another source of uncertainty in the outflow estimates is the ionization mechanisms in play, as collisional excitation may contribute. In fact, the low Lyα/He II ratio observed in the extended emission is not dissimilar to the one obtained in Scarlata et al. (2009) where, within another high-redshift ($z = 2.38$) system of Lyman alpha emitters, one of the sources displayed a comparably low ratio (Lyα/He II $= 2.2 \pm 1.0$) and the mechanism of origin was suspected to be accretion of cold gas onto the dark matter halo, resulting in collisional excitation.

Despite the large amount of energy injected into the host galaxy by the ionized outflow and the relativistic jets, TN J1049-1258 displays globally a very large SFR, although the companion galaxies might also contribute to the Herschel-measured flux. Rest frame far-infrared observations at high spatial resolution, e.g., those that can be produced by facilities such as the Atacama Large Millimeter/submillimeter Array, will be fundamental to obtain a more accurate estimate of the SFR in the host galaxy, and if possible, resolve its spatial distribution in a bid to better understand the interplay between jets, outflows, and gas reservoirs.

The possibility of outflows and more generally, jets, inducing star formation has been studied in both galactic (see Bicknell et al. 2000; Miley & De Breuck 2008; Capetti et al. 2022) and cosmological scales (Gilli et al. 2019), as well as simulations (Gaibler et al. 2012). As such, it is possible that the observed star formation from the RG is either induced or enhanced by the jet. Spatially resolved observations of cold molecular gas could answer questions such as where the star formation is occurring, whether jet-driven shocks are pressurizing gas bubbles in the intergalactic medium and causing fragmentation, or whether the expanding cocoon of the jet is inducing similar phenomena within the host galaxy itself. The cospatiality between the UV continuum and outflow suggests the former, though a mixture of both is not out of the question.

The presence of TN J1049-1258 inside a protocluster is within expectations. Studies have found that up to 75% of powerful HzRGs reside within these structures (Venemans et al. 2006). This is understandable considering that the powerful AGN responsible for this radio emission requires massive galaxies, which, in turn, inhabit rich, dense environments that act as fertile soil for cluster-like structures (Hatch et al. 2014). There is a great deal of relevance in protoclusters within the ΛCDM model, as they represent massive structures hypothetically linked by large dark matter halos: understanding how high-z and nearby galaxy clusters relate to each other is essential in unveiling the behavior and characteristics of dark matter. Their evolution through the cosmic ages as well as their relationship to powerful RLAGN, which likely become the

brightest cluster galaxies, are ongoing and widely studied topics within cosmology and high-redshift astrophysics.

Acknowledgments

Based on observations collected at the European Southern Observatory under ESO programme 108.22FU. CRA acknowledges the projects "Feeding and feedback in active galaxies", with reference PID2019-106027GB-C42, funded by MICINN-AEI/10.13039/501100011033, and 'Quantifying the impact of quasar feedback on galaxy evolution', with reference EUR2020-112266, funded by MICINN-AEI/10.13039/501100011033 and the European Union NextGenerationEU/PRTR.

Facilities: VLT:Yepun, Herschel, VLA, WISE.

ORCID iDs

Miguel Coloma Puga https://orcid.org/0009-0001-4945-5781
Barbara Balmaverde https://orcid.org/0000-0002-0690-0638
Alessandro Capetti https://orcid.org/0000-0003-3684-4275
Francesco Massaro https://orcid.org/0000-0002-1704-9850
Cristina Ramos Almeida https://orcid.org/0000-0001-8353-649X
George Miley https://orcid.org/0000-0003-2884-7214
Roberto Gilli https://orcid.org/0000-0001-8121-6177
Alessandro Marconi https://orcid.org/0000-0002-9889-4238

References

Ahn, S.-H. 2004, ApJL, 601, L25
Alexander, D. M., Swinbank, A. M., Smail, I., McDermid, R., & Nesvadba, N. P. H. 2010, MNRAS, 402, 2211
Antonucci, R. 1993, ARA&A, 31, 473
Astropy Collaboration, Price-Whelan, A. M., Sipőcz, B. M., et al. 2018, AJ, 156, 123
Astropy Collaboration, Robitaille, T. P., Tollerud, E. J., et al. 2013, A&A, 558, A33
Balmaverde, B., Marconi, A., Brusa, M., et al. 2016, A&A, 585, A148
Behrens, C., Dijkstra, M., & Niemeyer, J. C. 2014, A&A, 563, A77
Bicknell, G. V., Sutherland, R. S., van Breugel, W. J. M., et al. 2000, ApJ, 540, 678
Bornancini, C. G., Breuck, C. D., Vries, W. D., et al. 2007, MNRAS, 378, 551
Bouwens, R. J., Illingworth, G. D., Blakeslee, J. P., Broadhurst, T. J., & Franx, M. 2004, ApJL, 611, L1
Cano-Díaz, M., Maiolino, R., Marconi, A., et al. 2012, A&A, 537, L8
Capetti, A., Balmaverde, B., Tadhunter, C., et al. 2022, A&A, 657, A114
Cavagnolo, K. W., McNamara, B. R., Nulsen, P. E. J., et al. 2010, ApJ, 720, 1066
Chambers, K. C., Magnier, E. A., Metcalfe, N., et al. 2016, arXiv:1612.05560
Cicone, C., Feruglio, C., Maiolino, R., et al. 2012, A&A, 543, A99
Condon, J. J., Cotton, W. D., Greisen, E. W., et al. 1998, AJ, 115, 1693
Cresci, G., Mainieri, V., Brusa, M., et al. 2015, ApJ, 799, 82
Ferguson, H. C., Dickinson, M., Giavalisco, M., et al. 2004, ApJL, 600, L107
Fiore, F., Feruglio, C., Shankar, F., et al. 2017, A&A, 601, A143
Gaibler, V., Khochfar, S., Krause, M., & Silk, J. 2012, MNRAS, 425, 438
Gilli, R., Mignoli, M., Peca, A., et al. 2019, A&A, 632, A26
Griffin, M. J., Abergel, A., Abreu, A., et al. 2010, A&A, 518, L3
Hatch, N. A., Wylezalek, D., Kurk, J. D., et al. 2014, MNRAS, 445, 280
Hopkins, A. M. 2006, in ASP Conf. Ser. 380, At the Edge of the Universe: Latest Results from the Deepest Astronomical Surveys, ed. J. Afonso (San Francisco, CA: ASP), 423
Kerutt, J., Wisotzki, L., Verhamme, A., et al. 2022, A&A, 659, A183
Lacy, M., Baum, S. A., Chandler, C. J., et al. 2020, PASP, 132, 035001
Lagache, G., Cousin, M., & Chatzikos, M. 2018, A&A, 609, A130
Maiolino, R., Gallerani, S., Neri, R., et al. 2012, MNRAS: Letters, 425, L66
McCarthy, P. J. 1993, ARA&A, 31, 639
Miley, G., & De Breuck, C. 2008, A&ARv, 15, 67
Nenkova, M., Sirocky, M. M., Nikutta, R., Ivezić, Ž., & Elitzur, M. 2008, ApJ, 685, 160
Nesvadba, N. P. H., Breuck, C. D., Lehnert, M. D., et al. 2010, A&A, 525, A43
Osterbrock, D. E. 1989, Astrophysics of Gaseous Nebulae and Active Galactic Nuclei (Melville: Univ. Science Books), 408
Poglitsch, A., Waelkens, C., Geis, N., et al. 2010, A&A, 518, L2
Pouliasis, E., Georgantopoulos, I., Ruiz, A., et al. 2022, A&A, 658, A175
Price-Whelan, A. M., Lim, P. L., Earl, N., et al. 2022, ApJ, 935, 167
Ramos Almeida, C., Bischetti, M., García-Burillo, S., et al. 2022, A&A, 658, A155
Rodriguez Zaurin, J., Tadhunter, C. N., Rose, M., & Holt, J. 2013, MNRAS, 432, 138
Rupke, D. S. N., & Veilleux, S. 2011, ApJL, 729, L27
Rupke, D. S. N., & Veilleux, S. 2013, ApJL, 775, L15
Scarlata, C., Colbert, J., Teplitz, H. I., et al. 2009, ApJ, 706, 1241
Sobral, D., & Matthee, J. 2019, A&A, 623, A157
Speranza, G., Balmaverde, B., Capetti, A., et al. 2021, A&A, 653, A150
Speranza, G., Ramos Almeida, C., Acosta-Pulido, J. A., et al. 2022, A&A, 665, A55
Steidel, C. C., Erb, D. K., Shapley, A. E., et al. 2010, ApJ, 717, 289
Venemans, B. P., Röttgering, H. J. A., Miley, G. K., et al. 2006, A&A, 461, 823
Verhamme, A., Schaerer, D., & Maselli, A. 2006, A&A, 460, 397
Villar-Martín, M., Humphrey, A., Breuck, C. D., et al. 2007, MNRAS, 375, 1299
Weilbacher, P. M., Palsa, R., Streicher, O., et al. 2020, A&A, 641, A28
Wilkins, S. M., Gonzalez-Perez, V., Lacey, C. G., & Baugh, C. M. 2012, MNRAS, 427, 1490
Willott, C. J., Rawlings, S., Blundell, K. M., & Lacy, M. 1999, MNRAS, 309, 1017
Wright, E. L., Eisenhardt, P. R. M., Mainzer, A. K., et al. 2010, AJ, 140, 1868